Solar Energy xxx (xxxx) xxx–xxx

Contents lists available at ScienceDirect

Solar Energy

journal homepage: www.elsevier.com/locate/solener

An assessment of thermocline-control methods for packed-bed thermal-energy storage in CSP plants, Part 1: Method descriptions

L. Geissbühler[a], A. Mathur[b], A. Mularczyk[a], A. Haselbacher[a,*]

[a] Department of Mechanical and Process Engineering, ETH Zurich, 8092 Zurich, Switzerland
[b] Terrafore Technologies LLC, Minneapolis, MN 55402, USA

ARTICLE INFO

Keywords:
Thermal energy storage
Thermocline
Packed bed
Thermocline control

ABSTRACT

Thermocline thermal-energy storage (TES) suffers from so-called thermocline degradation, which refers to the flattening of temperature gradients in the TES with successive charging-discharging cycles. Thermocline degradation increases the variations of the heat-transfer fluid (HTF) outflow temperatures, decreases storage utilization factors, and increases specific TES material costs. Methods that prevent or reduce thermocline degradation by changing the operation of the storage are called thermocline-control (TCC) methods. The assessment of TCC methods is the main objective of this work. Three TCC methods that were chosen for this assessment are described in this paper. Two methods, based on either extracting or injecting HTF through ports, were derived from previously published methods while the third method, based on mixing multiple HTF streams, one of which is extracted through a port, is novel. In a companion paper (Geissbühler et al., Solar Energy, submitted 2018), the three TCC methods are assessed for air and molten salt as HTF using simulations of stand-alone storages as well as storages integrated into a concentrated solar power plant.

1. Introduction

Concentrated solar power (CSP) plants with thermal-energy storage (TES) offer dispatchable electricity from intermittent solar energy and are therefore expected to play an important role in the future electricity-generation mix. To reduce the levelized cost of the electricity generated by CSP plants, energy-efficient and cost-effective TES solutions are required. Two-tank molten-salt TES systems are currently the state-of-the-art and commercially implemented (Kuravi et al., 2013). In the last two decades, single-tank thermocline TES systems filled with a packed bed of low-cost filler material have attracted significant interest because they cost less than two-tank systems (Pacheco et al., 2002; Saeed Mostafavi Tehrani et al., 2017) and allow the use of ambient air as heat-transfer fluid (HTF) with applicability in a wider and higher temperature range (Zanganeh et al., 2012).

Thermocline TES systems are accompanied by several technical challenges, however. It was stated in Stekli et al. (2013) that “the biggest technoeconomic challenge of thermocline TES systems is temperature degradation”. Temperature degradation, also known as thermocline degradation, refers to the flattening of temperature gradients in the TES with successive charging-discharging cycles. Thermocline degradation has several negative consequences. One is an increase of the HTF outflow temperature during charging relative to the inflow temperature during discharging and a decrease of the HTF outflow temperature during discharging relative to the inflow temperature during charging. The maximum changes in the HTF outflow temperatures can be expressed in non-dimensional form as

$$\Delta\widetilde{T}_{c,\mathrm{out,max}} = \frac{T_{c,\mathrm{out,max}} - T_{d,\mathrm{in}}}{T_{c,\mathrm{in}} - T_{d,\mathrm{in}}}, \tag{1}$$

$$\Delta\widetilde{T}_{d,\mathrm{out,max}} = \frac{T_{c,\mathrm{in}} - T_{d,\mathrm{out,min}}}{T_{c,\mathrm{in}} - T_{d,\mathrm{in}}}, \tag{2}$$

where $T_{c,\mathrm{out,max}}$ is the maximum outflow temperature during charging, $T_{d,\mathrm{out,min}}$ is the minimum outflow temperature during discharging, $T_{c,\mathrm{in}}$ is the inflow temperature during charging, and $T_{d,\mathrm{in}}$ is the inflow temperature during discharging. The maximum outflow temperature change during charging is typically constrained by temperature restrictions of other CSP plant components such as piping, pumps, valves, and the solar receiver (Nithyanandam et al., 2012; Biencinto et al., 2014; Saeed Mostafavi Tehrani et al., 2017). Conversely, the maximum outflow temperature change during discharging is typically constrained by operating restrictions of the power block, in particular the desire for high efficiencies (Libby, 2010; Nithyanandam et al., 2012; Biencinto et al., 2014; Saeed Mostafavi Tehrani et al., 2017).

Another negative consequence of thermocline degradation is a

* Corresponding author.
E-mail address: haselbac@ethz.ch (A. Haselbacher).

https://doi.org/10.1016/j.solener.2018.12.015
Received 26 July 2018; Received in revised form 20 November 2018; Accepted 3 December 2018

Nomenclature

Abbreviations

CSP	concentrated solar power
HTF	heat-transfer fluid
PCM	phase-change material
TCC	thermocline control
TES	thermal-energy storage

Greek characters

Δ	difference, –
ζ	storage utilization factor, –
ξ	integration variable, –
ρ	density, kg/m^3
ϕ	volume fraction, –

Latin characters

A	area, m^2
c	specific heat capacity, J/kg K
E	thermal energy, J
H	height, m
i	index, –
m	mass, kg
p	pressure, Pa or bar
T	temperature, °C
t	time, s
x	axial coordinate, m

Subscripts

c	charging
d	discharging
f	fluid
s	solid
bot	bottom
ext	extracted
in	inflow
inj	injected
max	maximum
min	minimum
mix	mixing
out	outflow

Superscripts

–	average
·	flow rate
~	relative
*	threshold

limited utilization factor, which is defined as (Geyer et al., 1987; Dinter et al., 1991)

$$\zeta = \frac{\text{utilized storage capacity}}{\text{maximum storage capacity}}. \tag{3}$$

A quantitative definition is given by Eqs. (3)–(5) of the companion paper (Geissbühler et al., 2018). The smaller the utilization factor, the larger the specific material costs of the storage, i.e., the material costs per utilized capacity. Thus, thermocline degradation makes a storage both less efficient and more expensive, prompting the need for understanding the causes of thermocline degradation and finding methods to prevent or reduce it.

The causes of thermocline degradation are well known and include (1) limited convective heat transfer between the HTF and the storage material, (2) axial heat conduction and radiation, (3) mixing of HTF at different temperatures due to vortical flows, (4) mixing of HTF at different temperatures due to bypass flows adjacent to the container wall, and (5) heat exchange between the storage material/HTF and the storage container/insulation.

Much research has focused on finding methods that reduce thermocline degradation or mitigate its negative consequences, with the aim of decreasing the changes in the outflow temperatures or increasing the utilization factor. These research directions are not independent because the utilization factor and the changes in the outflow temperatures are related. Fig. 1 shows the utilization factor at the quasi-steady state, i.e., the state in which the thermoclines at the ends of successive charging and discharging phases become identical, as a function of the maximum allowed change in the outflow temperatures. The results were obtained from numerical simulations of a packed-bed storage that uses rocks as storage material and compressed air as HTF and has a maximum capacity of 1789 MW h$_{th}$. Clearly, the smaller the maximum allowed changes in the outflow temperatures, the smaller the utilization factor.

Methods that reduce thermocline degradation or mitigate at least some of its negative consequences can be classified as passive or active methods. Passive methods focus on the design of the storage, i.e., on its geometry and materials. Active methods, by contrast, focus on the operation of the storage, e.g., altering the flow of the HTF through the storage.

Passive methods include:

1. Increasing the height-to-diameter ratio of the storage while keeping its volume constant and/or increasing the heat-exchange surface area (e.g., by decreasing the particle diameter): This increases convective heat transfer and can decrease axial heat transfer at the expense of increased pumping work and increased thermal losses due to higher surface-to-volume ratios (Zanganeh et al., 2015). It should be noted that the storage height is usually limited for construction reasons (Libby, 2010).

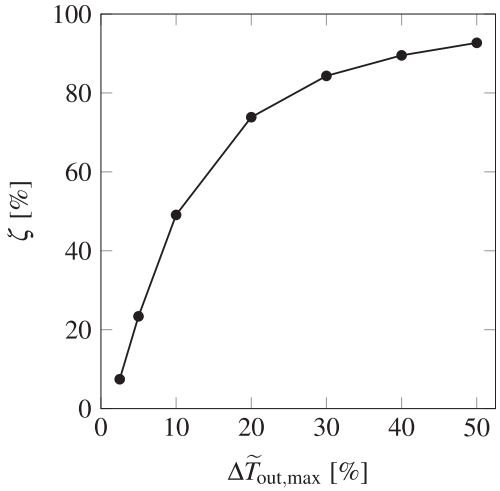

Fig. 1. Simulated utilization factor ζ as a function of the maximum allowed change in the outflow temperatures $\Delta\widetilde{T}_{\text{out, max}} = \Delta\widetilde{T}_{c,\text{out,max}} = \Delta\widetilde{T}_{d,\text{out,max}}$ for a packed-bed storage using rocks as storage material and compressed air as HTF and a maximum capacity of 1789 MW h$_{th}$. More information on the storage and the model with which the simulations were carried out are provided in the companion paper (Geissbühler et al., 2018).

2. Using phase-change materials (PCMs) at the top and/or at the bottom of the storage to stabilize the outflow temperatures (Hahne et al., 1991; Zanganeh et al., 2014; Galione et al., 2015; Geissbühler et al., 2016): Although encapsulated PCMs are typically significantly more expensive than low-cost sensible storage materials, cost reductions are possible due to the small amounts of PCM required for temperature stabilization (Geissbühler et al., 2016).
3. Cascaded latent storage (Farid, 1986; Farid and Kanzawa, 1989; Adebiyi et al., 1996; Michels and Pitz-Paal, 2007; Nithyanandam et al., 2012; Mathur et al., 2014): Using encapsulated PCMs that melt at different temperatures as filler materials can give higher utilization factors.
4. Cascaded thermochemical storage (Agrafiotis et al., 2016): Using filler materials that react at different temperatures can result in higher utilization factors. Material cyclability and costs can be issues.

Furthermore, the use of a floating barrier to separate hot and cold HTF was suggested (Wang et al., 1985; Copeland et al., 1985; Slocum et al., 2011; Lataperez and Blanco Lorenzo, 2011; Querol et al., 2012; Codd, 2015), but it is incompatible with the use of filler materials.[1] Increasing the height of the storage while keeping its diameter constant is also not considered as a method for decreasing the maximum changes in the outflow temperatures because it leads to a decrease of the utilization factor (Geissbühler et al., 2016).

Active methods, which are called thermocline-control (TCC) methods in this work, include:

1. Flushing: Periodically, the storage is discharged completely, i.e., the thermocline is expelled during discharging. One drawback is that part of the energy expelled during flushing is at low temperatures and might therefore be unusable for the power block. In CSP plants, the low-temperature energy could be used to protect against freezing of HTFs such as molten salts or synthetic oils (Biencinto et al., 2014).
2. Segmented storage (Crandall and Thacher, 2004): The packed bed is divided into multiple segments with ports between adjacent segments. The inlet port is switched to maintain thermal stratification in the case of variable inflow temperatures. During charging, ports whose temperature is higher than the inflow temperature are skipped. Similarly, during discharging, ports whose temperature is lower than the inflow temperature are skipped.
3. Sliding flow (Bindra and Bueno, 2016; Bindra et al., 2014; White et al., 2016; Howes et al., 2017): The packed bed is divided into multiple segments that are charged successively. Once a given segment is charged, the inlet and outlet ports are switched simultaneously to charge the next segment. The method was originally introduced to increase the exergy efficiency by partially decoupling the pressure drop from heat transfer. However, the method can also be used for TCC because it allows the thermocline to be confined to one segment. Thus, the more segments are used, the steeper the thermocline.
4. Extracting, upgrading, and returning (Mathur and Kasetty, 2013): The packed bed is again divided into multiple segments. The outlet port is switched and HTF is extracted at intermediate temperatures, upgraded, and returned to the top of the TES, leading to a local steepening of the thermocline.[2] This method is particularly interesting for CSP plants because the upgrade could be performed with thermal energy collected during periods of low insolation if the extracted temperature is high enough.
5. Siphoning (Walmsley et al., 2009): HTF is extracted at the position of the thermocline through a port while hot and cold HTF are supplied simultaneously from the top and bottom of the storage, respectively. Similar to flushing, the energy extracted during siphoning is at an intermediate temperature and might therefore be unusable for the power block.
6. Using a thermochemical section at the top of the storage to control the outflow temperature (Ströhle et al., 2017): The thermochemical storage material is encapsulated in tubes placed on top of the packed bed. By adjusting the pressure in the tubes, the heat released during discharging and therefore the outflow temperature of the HTF can be controlled.

Our interest is in reducing the negative effects of thermocline degradation in a sensible-heat storage containing a packed bed of a low-cost filler material such as rocks. Because we restrict our attention to sensible-heat storage, the only passive method of avoiding thermocline degradation is to adjust the height-to-diameter ratio and/or increase the heat-exchange surface area. In the following, we assume that this method was applied during the design of the storage and that TCC is required to further improve the storage performance.

To the best knowledge of the authors, no systematic assessment of TCC methods is available in the literature. Filling this gap is the main objective of the present work. Because the flushing and siphoning methods lead to potentially unusable low-temperature thermal energy, we focus on (1) the extracting, upgrading, and returning method, (2) a method based on injecting HTF that is derived from the sliding-flow method, and (3) a new method based on mixing HTF streams. In this paper, the three TCC methods are described in detail. In the companion paper (Geissbühler et al., 2018), the performance of the three methods is assessed for both air and molten salt as HTF using simulations of stand-alone storages as well as storages integrated into a CSP plant.

2. Description of TCC methods

We first present a brief description of the operation of a thermocline storage without TCC, which serves as the baseline for the assessment.

2.1. No TCC

The operation of a thermocline storage without TCC is depicted schematically in Fig. 2. In this and the subsequent schematic figures, the abscissa is the non-dimensional HTF temperature

$$\widetilde{T} = \frac{T - T_{d,\mathrm{in}}}{T_{c,\mathrm{in}} - T_{d,\mathrm{in}}} \tag{4}$$

and the ordinate is the non-dimensional axial coordinate $\widetilde{x} = x/H$, where H is the height of the storage. The dotted lines indicate $\widetilde{T}_{c,\mathrm{out,max}}$, the maximum non-dimensional HTF outflow temperature during charging, and $\widetilde{T}_{d,\mathrm{out,min}}$, the minimum non-dimensional HTF outflow temperature during discharging. The non-dimensional changes in the outflow temperatures defined by Eqs. (1) and (2) are also shown.

During the charging phase, the storage is supplied from the top with hot HTF, as indicated by the red arrows, at a temperature of $\widetilde{T}_{c,\mathrm{in}} = 1$. The thermocline represented by the dashed line moves downwards and cold HTF leaves the storage at the bottom, as indicated by the blue arrows. As long as the thermocline is not close to the bottom, the outflow temperature is close to $\widetilde{T}_{d,\mathrm{in}} = 0$. As the thermocline approaches the bottom, however, the outflow temperature begins to increase. The charging phase is terminated when the increase in the outflow temperature reaches the specified limit of $\Delta\widetilde{T}_{c,\mathrm{out,max}}$.

Conversely, during the discharging phase, the storage is supplied from the bottom with cold HTF at a temperature of $\widetilde{T}_{d,\mathrm{in}} = 0$. The thermocline moves upwards and hot HTF leaves the storage at the top. As long as the thermocline is not close to the top, the outflow

[1] The barrier reduces axial radiative and conductive heat transfer. Achieving an effective seal between the storage walls and the barrier is challenging.

[2] We use "steepening" to indicate increases in the magnitude of the temperature gradient $|\mathrm{d}T/\mathrm{d}x|$, where x is the axial coordinate.

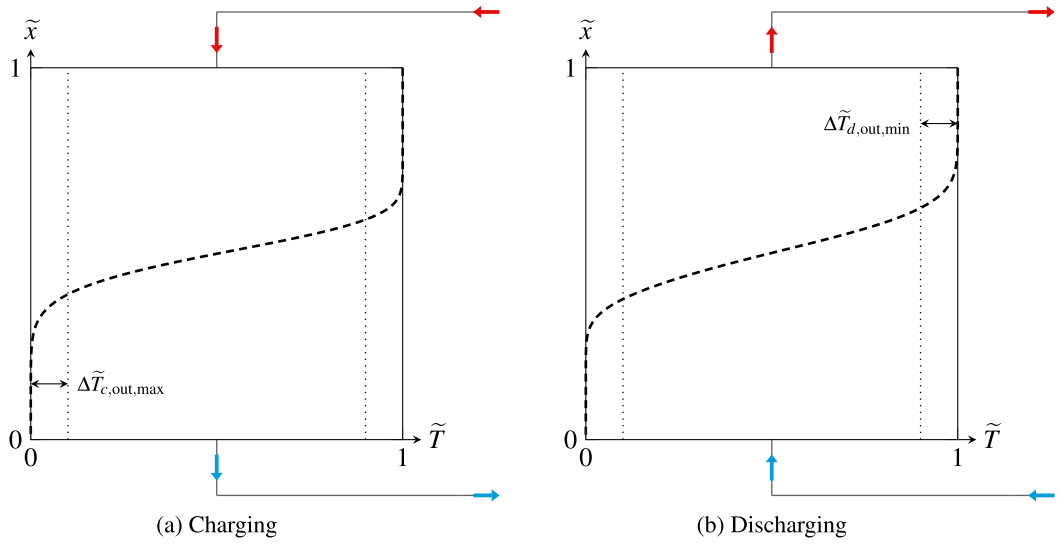

Fig. 2. Schematic depiction of the operation of a thermocline storage without TCC during charging and discharging. The dashed lines represent the thermoclines halfway through the charging and discharging phases. The dotted lines indicate $\widetilde{T}_{c,\mathrm{out,max}}$, the maximum HTF outflow temperature during charging, and $\widetilde{T}_{d,\mathrm{out,min}}$, the minimum HTF outflow temperature during discharging. Red arrows indicate the flow direction of HTF with temperatures of $\widetilde{T} \geqslant \widetilde{T}_{d,\mathrm{out,min}}$. Blue arrows indicate the flow direction of HTF with temperatures of $\widetilde{T} \leqslant \widetilde{T}_{c,\mathrm{out,max}}$. (For interpretation of the references to colour in this figure legend, the reader is referred to the web version of this article.)

temperature is close to $\widetilde{T}_{c,\mathrm{in}} = 1$. As the thermocline reaches the top, however, the outflow temperature starts to decrease. The discharging phase is terminated when the decrease in the outflow temperature reaches the specified limit of $\Delta\widetilde{T}_{d,\mathrm{out,min}}$. [3]

2.2. Extracting method

The first method investigated in this work is the extracting, upgrading, and returning method (Mathur and Kasetty, 2013); for brevity, we refer to it as the extracting method. We assume that the extracted HTF is upgraded in the receiver of the CSP plant and returned to the top of the storage.

The operation of the storage with the extracting method is explained in Fig. 3. To simplify the explanation of the method, we restrict our attention to the case in which HTF is extracted through only one port that is located at the mid-height of the storage. The restriction to one port is lifted in the assessment of the TCC methods in the companion paper (Geissbühler et al., 2018).

At the beginning of the charging phase, hot HTF is supplied to the storage at the top and extracted through the port, see Fig. 3(a). The solid lines indicate the thermoclines produced by the extracting method just before port switching. The dashed lines show the thermoclines produced without TCC at the same instant. As soon as the HTF outflow temperature at the port reaches $\widetilde{T}_{c,\mathrm{out,max}}$, the HTF outlet is switched from the port to the bottom, see Fig. 3(b). (If there are multiple ports, the outlet is switched to the port located immediately below that through which HTF is being extracted.)

The operation during the discharging phase is analogous. Cold HTF is supplied to the storage from the bottom and extracted through the port, see Fig. 3(c). Once the HTF outflow temperature at the port drops below $\widetilde{T}_{d,\mathrm{out,min}}$, the HTF outlet is switched to the top, see Fig. 3(d). (If there are multiple ports, the outlet is switched to the port located immediately above that through which HTF is being extracted.)

[3] In this description, we have assumed that the height and diameter of the storage are given and that the maximum allowed changes in the outflow temperatures determine the durations of the charging and discharging phases. If the durations of the charging and discharging phases are given instead, the maximum allowed changes in the outflow temperatures can be used to determine the height and diameter of the storage.

Comparing the solid and dashed lines in Fig. 3 shows that the extracting method does indeed lead to a steepening of the thermocline, but also suggests that the impact of the method is limited. The limited impact is explained by the fact that the thermoclines shown in the figure represent simulation results during the first charging and discharging phases. As shown in the companion paper (Geissbühler et al., 2018), at the quasi-steady state the impacts of all the TCC methods investigated in this work are substantial.

2.3. Injecting method

As implied by its name, the injecting method can be viewed as the opposite of the extracting method: Instead of extracting HTF, it is injected into the storage. The injecting method is derived from the sliding-flow method (Bindra and Bueno, 2016; Bindra et al., 2014; White et al., 2016; Howes et al., 2017). The operation of the storage with the injecting method and one port is illustrated in Fig. 4, where the lines have the same meanings as in Fig. 3.

At the beginning of the charging phase, hot HTF enters the storage from the top and cold HTF leaves from the bottom as shown in Fig. 4(a), just as without TCC. When certain switching criteria that will be discussed below are fulfilled, the supply of hot HTF is switched from the top to the port, see Fig. 4(b), where the arrows indicate the flow of the HTF after switching. In Fig. 4(a) it can be seen that the HTF temperature at the port position is significantly lower than $\widetilde{T}_{d,\mathrm{out,min}}$. In Fig. 4(b), some time after switching, the HTF temperature at the port position has risen to $\widetilde{T}_{c,\mathrm{in}} = 1$.

The operation of the storage during the discharging phase is analogous. Prior to port switching, as indicated in Fig. 4(c), cold HTF enters the storage from the bottom and hot HTF leaves at the top just as without TCC. When the switching criteria are satisfied, the supply of hot HTF is switched from the bottom to the port. Some time after switching, the HTF temperature at the position of the port has dropped to $\widetilde{T}_{d,\mathrm{in}} = 0$, see Fig. 4(d).

Two observations can be made about Fig. 4(d). First, by comparing the solid and dashed lines, it becomes clear that the injecting method leads to a steepening of the thermocline. Second, the thermocline exhibits an oscillation near the top of the storage. This oscillation is caused by switching the supply of hot HTF from the top to the port during the charging phase, see Fig. 4(b). Axial dispersion (due to

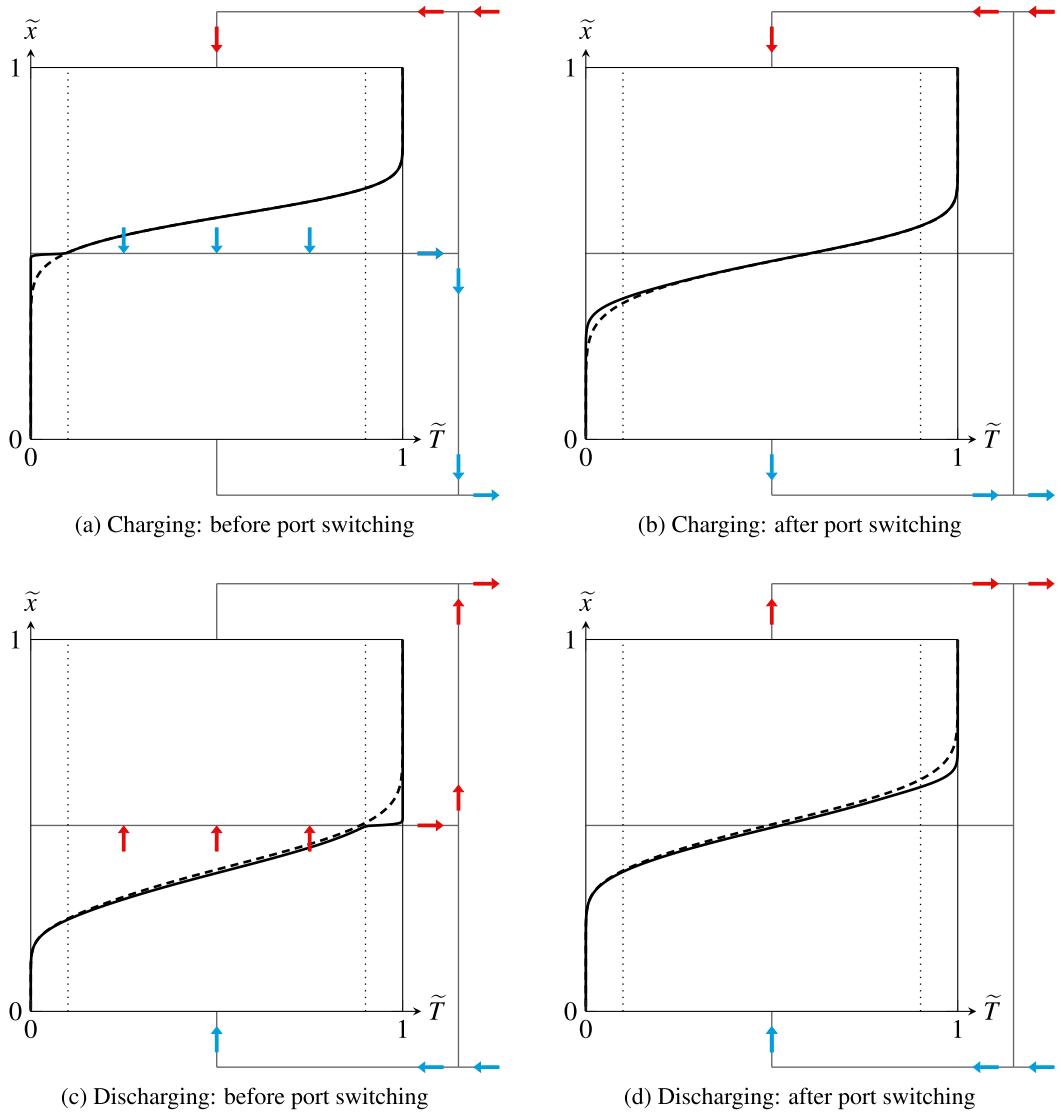

(a) Charging: before port switching

(b) Charging: after port switching

(c) Discharging: before port switching

(d) Discharging: after port switching

Fig. 3. Schematic depiction of the operation of a thermocline storage with the extracting method using one port located at the storage mid-height. The solid lines represent the thermoclines resulting from the extracting method at representative instants during the charging and discharging phases. The dashed lines represent the thermoclines without TCC at the same instants. The other lines and arrows are explained in the caption of Fig. 2.

limited convective heat transfer, conduction, and radiation) reduces the amplitude and increases the axial extent of the oscillation. As the oscillation approaches the top of the storage during discharging, $\widetilde{T}_{d,\mathrm{out}}$ becomes oscillatory. It should be noted that during the charging phase that follows the discharging phase depicted in Fig. 4(d), $\widetilde{T}_{c,\mathrm{out}}$ will be oscillatory also.

Ensuring that the amplitudes of the oscillations in $\widetilde{T}_{c,\mathrm{out}}$ and $\widetilde{T}_{d,\mathrm{out}}$ remain below $\Delta\widetilde{T}_{c,\mathrm{out,max}}$ and $\Delta\widetilde{T}_{d,\mathrm{out,min}}$, respectively, is the objective of the port-switching criteria. Finding effective port-switching criteria is not straightforward. The criteria used in this work are based on the ratio of two thermal energies between the current inlet and the proximate (downstream) port, where "inlet" refers to either the usual inlets at the top and bottom of the storage or a port. In the following, the axial positions of the current inlet and the proximate port are denoted by x_i and x_{i+1}. The first thermal energy is the actual thermal energy stored between the current inlet and the proximate port,

$$E_i(t) = \int_{x_i}^{x_{i+1}} A(x) \int_{T_{d,\mathrm{in}}}^{T(x,t)} [(1-\phi_s)\rho_f(\xi)c_{p,f}(\xi) + \phi_s\rho_s(\xi)c_s(\xi)]\,\mathrm{d}\xi\,\mathrm{d}x, \tag{5}$$

where $A(x)$ is the cross-sectional area of the TES, ϕ_s is the solid volume fraction of the packed bed, ρ_f is the density of the HTF, ρ_s is the density of the filler material, is the specific heat capacity at constant pressure of the HTF, and c_s is the specific heat capacity of the filler material. The second thermal energy is the so-called threshold thermal energy. During the charging phase, the threshold thermal energy is defined as

$$E^*_{c,i} = \int_{x_i}^{x_{i+1}} A(x) \int_{T_{d,\mathrm{in}}}^{T_{c,\mathrm{in}}-\Delta T_{\mathrm{inj}}} [(1-\phi_s)\rho_f(\xi)c_{p,f}(\xi) + \phi_s\rho_s(\xi)c_s(\xi)]\,\mathrm{d}\xi\,\mathrm{d}x, \tag{6}$$

where ΔT_{inj} is a specified temperature difference. The threshold energy can be interpreted as the net thermal energy between the temperatures $T_{d,\mathrm{in}}$ and $T_{c,\mathrm{in}} - \Delta T_{\mathrm{inj}}$ stored in the volume between the current inlet and the proximate port. Using these two thermal energies, the port-switching criterion during the charging phase can be expressed as

$$\frac{E_i(t)}{E^*_{c,i}} \geqslant 1. \tag{7}$$

This criterion is illustrated in Fig. 5(a), where $E_i(t)$ and $E^*_{c,i}$ are indicated by the hatched and green areas, respectively. The solid line shows the thermocline at the instant when the criterion is just met, i.e., when $E_i(t)/E^*_{c,i} = 1$.

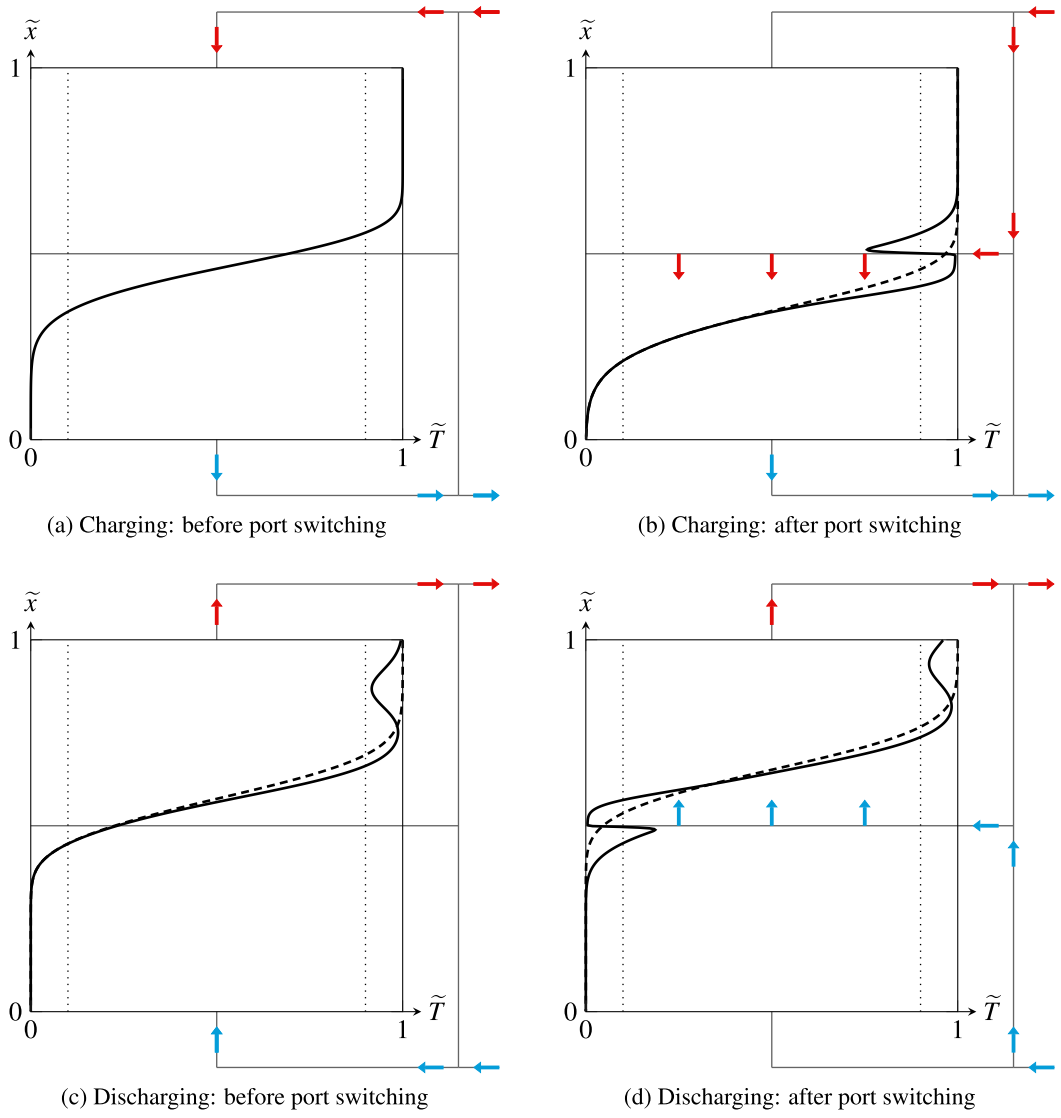

(a) Charging: before port switching

(b) Charging: after port switching

(c) Discharging: before port switching

(d) Discharging: after port switching

Fig. 4. Schematic depiction of the operation of a thermocline storage with the injecting method using one port located at the storage mid-height. The solid lines represent the thermoclines resulting from the injecting method during the charging and discharging phases. The dashed lines represent the thermoclines without TCC at the same instants. The other lines and arrows are explained in the caption of Fig. 2.

Conversely, during the discharging phase the threshold energy is defined as

$$E^*_{d,i} = \int_{x_i}^{x_{i+1}} A(x) \int_{T_{d,\mathrm{in}}}^{T_{d,\mathrm{in}}+\Delta T_{\mathrm{inj}}} [(1-\phi_s)\rho_f(\xi)c_{p,f}(\xi) + \phi_s\rho_s(\xi)c_s(\xi)]\,\mathrm{d}\xi\,\mathrm{d}x \tag{8}$$

and the port-switching criterion is

$$\frac{E_i(t)}{E^*_{d,i}} \leqslant 1, \tag{9}$$

as illustrated in Fig. 5(b).

For constant cross-sectional area, solid volume fraction, densities, and specific heat capacities, Eqs. (7) and (9) simplify to $\overline{T}_i \geqslant T_{c,\mathrm{in}} - \Delta T_{\mathrm{inj}}$ and $\overline{T}_i \leqslant T_{d,\mathrm{in}} + \Delta T_{\mathrm{inj}}$, respectively, where $\overline{T}_i$ is the average temperature between x_i and x_{i+1}. In Eqs. (6) and (8), we have assumed for simplicity that the temperature differences ΔT_{inj} are identical. The value of ΔT_{inj} that results in a desired utilization factor depends on the rate of thermocline degradation and on the number of ports and must either be chosen a priori or be determined by simulations.

2.4. Mixing method

The operation of the storage with the novel mixing method and one port during the charging phase is illustrated in Fig. 6. At the beginning of the charging phase, HTF is supplied to the storage from the top and extracted from the port, just like for the extracting method, see Fig. 6(a). The extracting and mixing methods differ once the temperature of the HTF extracted through the port exceeds $\widetilde{T}_{c,\mathrm{out,max}}$. Rather than switching the outlet to the bottom of the storage, HTF is extracted simultaneously from the port and the bottom, see Fig. 6(b).[4] The two extracted streams are mixed such that the temperature of the mixed HTF equals $\widetilde{T}_{c,\mathrm{out,max}}$. For the case of only one port, the time-dependent mass flow rate at the bottom of the storage, denoted by $\dot{m}_{\mathrm{bot}}(t)$, is determined from

[4] As for the other methods, if there are multiple ports, first the proximate port is used instead of that at the bottom.

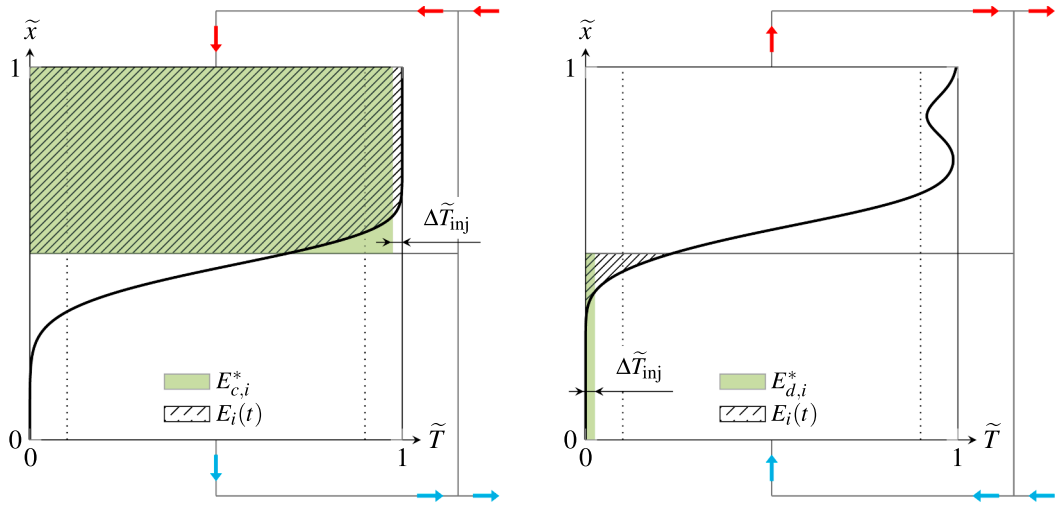

(a) Charging (b) Discharging

Fig. 5. Schematic depiction of the port-switching criterion with the injecting method during charging (left) and discharging (right). The schematic shows the instant when the criterion is just met, i.e., when $E_i(t)/E^*_{c,i} = 1$ during charging and $E_i(t)/E^*_{d,i} = 1$ during discharging. Note that the highlighted areas correspond only qualitatively to the respective energies, see Eqs. (5), (6), and (8) for the precise expressions.

$$(\dot{m}_{\text{top}} - \dot{m}_{\text{bot}}(t)) \int_{T_{\text{ref}}}^{T_{\text{ext}}(t)} c_{p,f}(\xi)\,d\xi + \dot{m}_{\text{bot}}(t) \int_{T_{\text{ref}}}^{T_{\text{c,out}}(t)} c_{p,f}(\xi)\,d\xi = \dot{m}_{\text{top}} \int_{T_{\text{ref}}}^{T_{\text{c,out,max}}} c_{p,f}(\xi)\,d\xi,$$

where $\dot{m}_{\text{top}}$ is the mass flow rate supplied to the storage at the top and T_{ref} is an arbitrary reference temperature. If the specific heat is constant, one obtains

$$\frac{\dot{m}_{\text{bot}}(t)}{\dot{m}_{\text{top}}} = \frac{T_{\text{ext}}(t) - T_{\text{c,out,max}}}{T_{\text{ext}}(t) - T_{\text{c,out}}(t)}.$$

Because $\dot{m}_{\text{bot}}(t)/\dot{m}_{\text{top}} \leqslant 1$, the part of the thermocline below the port moves slower than that above the port, thereby contributing to the steepening of the thermocline as a whole.

During discharging with the mixing method, the storage is operated in an analogous manner, see Fig. 6(c) and (d). Instead of reducing the mass flow below the port, the mass flow above the port is reduced. Comparing the dashed and the solid lines indicates that the mixing method steepens the thermocline.

Fig. 7 shows the temporal variations of the extracted non-dimensional mass flow rates and HTF temperatures at the port, the top and the bottom during the first charging and discharging phases. For completeness, the constant non-dimensional mass flow rates and HTF temperatures at the inlets are also shown. The blue and red backgrounds indicate that the outflow temperatures at a given outlet satisfy the restrictions on the maximum/minimum outflow temperatures during charging/discharging, respectively, and therefore these outlets are referred to as primary outlets. Conversely, the yellow background signals that the outflow temperatures at a given outlet violate the restrictions and therefore the outlet is termed a secondary outlet. The figure shows clearly how the primary and secondary outlets are switched and the corresponding mass flow rates are controlled such that the temperature of the mixed outlet streams do not rise above $\widetilde{T}_{\text{c,out,max}}$ or fall below $\widetilde{T}_{\text{d,out,min}}$ during charging and discharging, respectively. At the beginning of the charging/discharging phase the temperature is not controlled to the limit because the thermocline has not yet arrived at the port and therefore no outlet temperature control is possible using the port and the bottom/top outlet. The times when the outflow temperatures during the first charging and discharging phases start to be controlled are $\widetilde{t} \approx 0.5$ and $\widetilde{t} \approx 0.25$, respectively. These times differ for two main reasons: First, at the start of the first charging phase the storage is assumed to be completely discharged and therefore the thermocline is particularly steep early in the first charging phase. Consequently, the thermocline reaches the port later compared to the operation at the quasi-steady state when the thermocline will be less steep. By contrast, at the beginning of the first discharging phase the thermocline steepness is already quite close to that at the quasi-steady state and therefore the thermocline reaches the port earlier. The second reason relates to the storage geometry, which has a truncated cone shape with a larger diameter at the top, see the companion paper (Geissbühler et al., 2018). Consequently, more energy per unit height can be stored at the top than at the bottom, leading to a thermocline that moves more slowly and is steeper at the top than at the bottom, which implies that the thermocline reaches the port later during charging than during discharging also at the quasi-steady state.

If there are multiple ports, the two active outlets through which HTF is extracted during charging are chosen as follows: The primary outlet is the one closest downstream of the thermocline and that has a temperature that is still below $T_{\text{c,out,max}}$. The secondary outlet is the one immediately upstream of the primary outlet, where $T \geqslant T_{\text{c,out,max}}$. If the secondary outlet would correspond to the inlet, then only the primary outlet is active. During discharging, the two active outlets are chosen in an analogous manner.g.

The mixing method assessed in this work can potentially be extended in two ways. First, it is possible to eliminate the rise and fall of the outflow temperatures produced by the mixing method by combining it with bypassing of the TES, see (Schmidt and Willmott, 1981, pp. 160–162; El-Halwagi and El-Rifai, 1990). Bypassing is based on mixing the inflow and outflow streams to control the temperature of the mixed outflow stream. In combination with the mixing method, bypassing would need to be applied only at the beginning of the charging and discharging phases. Additionally, the combination would allow controlling the outflow temperature to any desired outflow temperature profile, such as, e.g., a temperature ramp. In this study, bypassing was not considered as it does not steepen the thermocline. The second extension is that the restriction of keeping the inlet at the top/bottom during the entire charging/discharging phase could be lifted. To decrease the pressure drop, the inlet could be switched also, similar to the injecting method.

2.5. Discussion

Combining the extracting and injecting methods would result in a method with some similarities to the sliding-flow method. There are

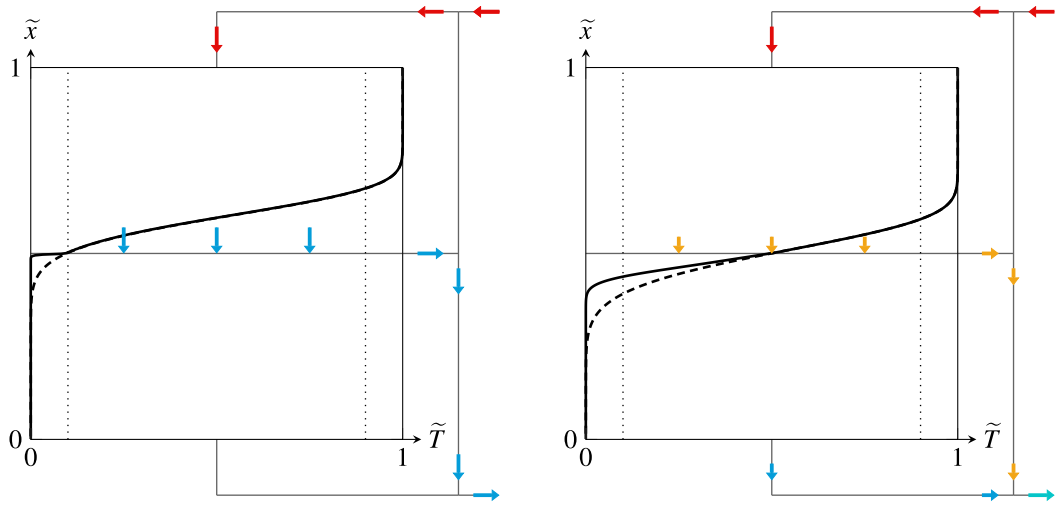

(a) Charging: before port switching

(b) Charging: after port switching

(c) Discharging: before port switching

(d) Discharging: after port switching

Fig. 6. Schematic depiction of the operation of a thermocline storage with the mixing method using one port located at the storage mid-height. The solid lines represent the thermoclines resulting from the mixing method during the charging and discharging phases. The dashed lines represent the thermoclines without TCC at the same instants. Yellow arrows indicate the flow direction of HTF with temperatures of $\widetilde{T}_{c,\mathrm{out,max}} < \widetilde{T} < \widetilde{T}_{d,\mathrm{out,min}}$. The other lines and arrows are explained in the caption of Fig. 2. (For interpretation of the references to colour in this figure legend, the reader is referred to the web version of this article.)

several important differences between the sliding-flow method and a combined extracting/injecting method, however. First, the port-switching criterion used in the sliding-flow method is based on the temperature rather than on the ratio of thermal energies as in Eqs. (7) and (9). Second, the port-switching criterion as described in Bindra et al. (2014) corresponds to $\Delta T_{\mathrm{inj}} = 0$, which leads to thermoclines and utilization factors that are almost identical to those of the extracting method. Third, in the sliding-flow method the injection and extraction ports are switched simultaneously. Fourth, the sliding-flow method as described in Bindra et al. (2014) operates with two active ports that straddle an inactive port. Finally, and most importantly, it is unlikely that using a combined extracting/injecting method would further steepen the thermocline compared to using either the extracting or the injecting method. To see why, consider the thermocline shown in Fig. 4(b). If the thermocline in the subsequent discharging phase would be extracted as in Fig. 3(c), we would extract precisely that part of the thermocline that had been steepened in the previous charging phase, and thereby actually decrease the thermocline steepness.

3. Summary

Thermocline degradation has the disadvantages of (1) increases/decreases of the HTF outflow temperatures during charging/discharging, respectively and (2) limited utilization factors. These disadvantages are coupled because the smaller the allowed increases/decreases in the HTF outflow temperatures, the smaller the utilization factor and vice versa. Smaller utilization factors, in turn, increase the specific material cost of the TES. The incentive to preventing or reducing thermocline degradation is therefore clear.

Methods that prevent thermocline degradation can be classified as passive or active methods. Passive methods focus on the design of the TES, whereas active methods, called TCC methods in this work, focus on the operation of the TES. Three TCC methods were assessed in this work. The description of the methods is the focus of this paper. The assessment of the methods is the subject of a companion paper (Geissbühler et al., 2018).

Common to the three TCC methods are so-called ports, which are openings in the TES that are not located at the top and bottom like the usual inlets and outlets and through which HTF can be either extracted

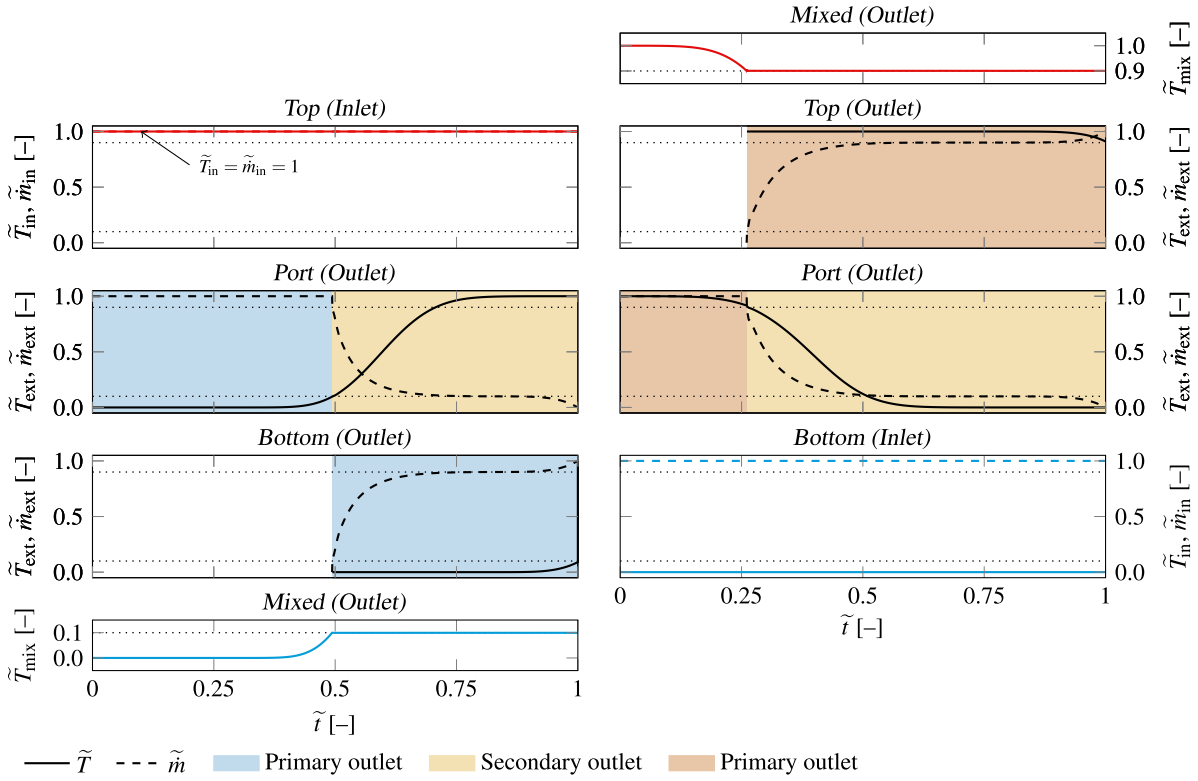

Fig. 7. Inflow/outflow temperatures (solid lines) and mass flow rates (dashed lines) at the inlets/outlets as a function of non-dimensional time during the first charging (left) and discharging (right) phases for the mixing method using one port located at the storage mid-height. The dotted lines correspond to $\widetilde{T}_{c,out,max}$ and $\widetilde{T}_{d,out,min}$, respectively. The mass flow rates are normalized with the inflow mass flow rates.

or injected. The first method, referred to as the extracting method, is based on extracting HTF through the ports. By extracting HTF as the thermocline moves past the port, a local steepening of the thermocline is effected. The second method is referred to as the injecting method and is based on injecting HTF through the ports. By injecting HTF when certain switching criteria are met, the thermocline can be steepened locally. The third method is novel and referred to as the mixing method. It is based on extracting HTF from two outlets simultaneously, at least one of which is a port. The two outlet streams are mixed such that temperature of the mixed stream is equal to a specified outflow temperature. In contrast to the other two methods, the mixing method allows not only for steepening of the thermocline but also for a controllable/constant outflow temperature.

Acknowledgment

Funding by the Swiss Commission for Technology and Innovation through the Swiss Competence Center for Energy Research on Heat and Electricity Storage is gratefully acknowledged. The authors are grateful to Aldo Steinfeld for his support.

References

Adebiyi, G., Hodge, B., Steele, W., Jalalzadeh-Azar, A., Nsofor, E., 1996. Computer simulation of a high-temperature thermal energy storage system employing multiple families of phase-change storage materials. J. Energy Resour. Technol. 118, 102–111.

Agrafiotis, C., Roeb, M., Sattler, C., 2016. Exploitation of thermochemical cycles based on solid oxide redox systems for thermochemical storage of solar heat. part 4, Screening of oxides for use in cascaded thermochemical storage concepts. Sol. Energy 139, 695–710.

Biencinto, M., Bayón, R., Rojas, E., González, L., 2014. Simulation and assessment of operation strategies for solar thermal power plants with a thermocline storage tank. Sol. Energy 103, 456–472.

Bindra, H., Bueno, P., 2016. Optimum process design of packed bed type thermal storage systems and other applications. US Patent App. 14/234,286.

Bindra, H., Bueno, P., Morris, J., 2014. Sliding flow method for exergetically efficient packed bed thermal storage. Appl. Therm. Eng. 64 (1), 201–208.

Codd, D., 2015. Experimental investigation of divider plate assisted thermocline storage. In: ASME 2015 9th International Conference on Energy Sustainability Collocated with the ASME 2015 Power Conference, the ASME 2015 13th International Conference on Fuel Cell Science, Engineering and Technology, and the ASME 2015 Nuclear Forum. American Society of Mechanical Engineers pp. V001T05A002–V001T05A002.

R. Copeland, 1985. Method and apparatus for operating an improved thermocline storage unit. US Patent 4,523,629.

Crandall, D., Thacher, E., 2004. Segmented thermal storage. Sol. Energy 77 (4), 435–440.

Dinter, F., Geyer, M., Tamme, R., 1991. Thermal Energy Storage for Commercial Applications. Springer-Verlag, Berlin.

El-Halwagi, A., El-Rifai, M., 1990. Simulation of variable flow fluidized bed heat regenerators. Chem. Eng. Commun. 91 (1), 235–240.

Farid, M., 1986. Solar energy storage with phase change. J. Sol. Energy Res. 4 (11).

Farid, M., Kanzawa, A., 1989. Thermal performance of a heat storage module using pcm's with different melting temperatures, mathematical modeling. J. Sol. Energy Eng. 111 (2), 152–157.

Galione, P., Pérez-Segarra, C., Rodríguez, I., Oliva, A., Rigola, J., 2015. Multi-layered solid-PCM thermocline thermal storage concept for CSP plants. Numerical analysis and perspectives. Appl. Energy 142, 337–351.

Geissbühler, L., Mathur, A., Mularczyk, A., Haselbacher, A., Steinfeld, A., 2018. An assessment of thermocline-control methods for packed-bed thermal-energy storage in CSP plants, Part 2, Assessment strategy and results (in preparation).

Geissbühler, L., Kolman, M., Zanganeh, G., Haselbacher, A., Steinfeld, A., 2016. Analysis of industrial-scale high-temperature combined sensible/latent thermal energy storage. Appl. Therm. Eng. 101, 657–668.

Geyer, M., Bitterlich, W., Werner, K., 1987. The dual medium storage tank at the IEA/SSPS project in Almeria (Spain); Part I, Experimental validation of the thermodynamic design model. J. Sol. Energy Eng. 109 (3), 192–198.

Hahne, E., Taut, U., Gross, U., 1991. Salt ceramic thermal energy storage for solar thermal central receiver plants. Solar World Cong. 2, 1937–1941.

Howes, J., MacNaghten, J., Hunt, R., 2017. Layered thermal store with selectively alterable gas flow path. US Patent 9,658,004.

Kuravi, S., Trahan, J., Goswami, Y., Rahman, M., Stefanakos, E., 2013. Thermal energy storage technologies and systems for concentrating solar power plants. Prog. Energy Combust. Sci. 39 (4), 285–319.

Lataperez, J., Blanco Lorenzo, J., 2011. Dual thermal energy storage tank. US Patent App. 13/001,759.

Libby, C., 2010. Solar Thermocline Storage System–Preliminary Design Study. Electric Power Research Institute, Palo Alto, California.

Mathur, A., Kasetty, R., 2013. Thermal energy storage system comprising optimal thermocline management. US Patent 8,554,377.

Mathur, A., Kasetty, R., Oxley, J., Mendez, J., Nithyanandam, K., 2014. Using

encapsulated phase change salts for concentrated solar power plant. Energy Proc. 49, 908–915.
Michels, H., Pitz-Paal, R., 2007. Cascaded latent heat storage for parabolic trough solar power plants. Sol. Energy 81 (6), 829–837.
Nithyanandam, K., Pitchumani, R., Mathur, A., 2012. Analysis of a latent thermocline energy storage system for concentrating solar power plants. In: ASME 2012 6th International Conference on Energy Sustainability collocated with the ASME 2012 10th International Conference on Fuel Cell Science, Engineering and Technology. American Society of Mechanical Engineers, pp. 519–528.
Pacheco, J., Showalter, S., Kolb, W., 2002. Development of a molten-salt thermocline thermal storage system for parabolic trough plants. J. Sol. Energy Eng. 124, 153–159.
Querol, P., Olano, J., Pereña, A., Velasco, T., Arevalo, J., Lata, J., 2012. Single tank thermal storage prototype. In: Proceedings of the 12th SolarPACES International Conference.
Saeed Mostafavi Tehrani, S., Taylor, R., Nithyanandam, K., Shafiei Ghazani, A., 2017. Annual comparative performance and cost analysis of high temperature, sensible thermal energy storage systems integrated with a concentrated solar power plant. Sol. Energy 153, 153–172.
Schmidt, F.W., Willmott, A.J., 1981. Thermal Energy Storage and Regeneration. Hemisphere Publishing Corporation, Washington.
Slocum, A., Buongiorno, J., Forsberg, C., Codd, D., Paxson, A., 2011. Concentrated solar power system. WO Patent App. PCT/US2010/049,474.
Stekli, J., Irwin, L., Pitchumani, R., 2013. Technical challenges and opportunities for concentrating solar power with thermal energy storage. J. Thermal Sci. Eng. Appl. 5 (2), 021011.
Ströhle, S., Haselbacher, A., Jovanovic, Z., Steinfeld, A., 2017. Upgrading sensible-heat storage with a thermochemical storage section operated at variable pressure: an effective way toward active control of the heat-transfer fluid outflow temperature. Appl. Energy 196, 51–61.
Walmsley, M., Atkins, M., Riley, J., 2009. Thermocline management of stratified tanks for heat storage. In: Proceedings of 12th International Conference on Process Integration, Modelling and Optimisation for Energy Saving and Pollution Reduction.
Wang, K.Y., West, R.E., Kreith, F., Lynn, P., 1985. High-temperature sensible-heat storage options. Energy 10 (10), 1165–1175.
White, A., McTigue, J., Markides, C., 2016. Analysis and optimisation of packed-bed thermal reservoirs for electricity storage applications. Proc. Inst. Mech. Eng., Part A, J. Power Energy 230 (7), 739–754.
Zanganeh, G., Pedretti, A., Zavattoni, S., Barbato, M., Steinfeld, A., 2012. Packed-bed thermal storage for concentrated solar power – pilot-scale demonstration and industrial-scale design. Sol. Energy 86 (10), 3084–3098.
Zanganeh, G., Commerford, M., Haselbacher, A., Pedretti, A., Steinfeld, A., 2014. Stabilization of the outflow temperature of a packed-bed thermal energy storage by combining rocks with phase change materials. Appl. Therm. Eng. 70 (1), 316–320.
Zanganeh, G., Pedretti, A., Haselbacher, A., Steinfeld, A., 2015. Design of packed bed thermal energy storage systems for high-temperature industrial process heat. Appl. Energy 137, 812–822.